ACS APPLIED MATERIALS & INTERFACES

Research Article

www.acsami.org

Iridium Oxide–Polymer Nanocomposite Electrode Materials for Water Oxidation

Youssef Lattach, Juan Francisco Rivera, Tahya Bamine, Alain Deronzier, and Jean-Claude Moutet*

Département de Chimie Moléculaire, UMR CNRS-5250, Institut de Chimie Moléculaire de Grenoble, Université Joseph Fourier Grenoble1 , FR CNRS-2607, BP 53, 38041, Grenoble Cedex 9, France

Supporting Information

ABSTRACT: Nanocomposite anode materials for water oxidation have been readily synthesized by electrodeposition of iridium oxide nanoparticles into poly(pyrrole-alkylammonium) films, previously deposited onto carbon electrodes by oxidative electropolymerization of a pyrrole-alkylammonium monomer. The nanocomposite films were characterized by electrochemistry, transmission electron microscopy, and atomic force microscopy. They showed an efficient electrocatalytic activity toward the oxygen evolution reaction. Data from Tafel plots have demonstrated that the catalytic activity of the iridium oxide nanoparticles is maintained following their inclusion in the polymer matrix. Bulk electrolysis of water at carbon foam modified electrodes have shown that the iridium oxide–polymer composite presents a higher catalytic activity and a better operational stability than regular oxide films.

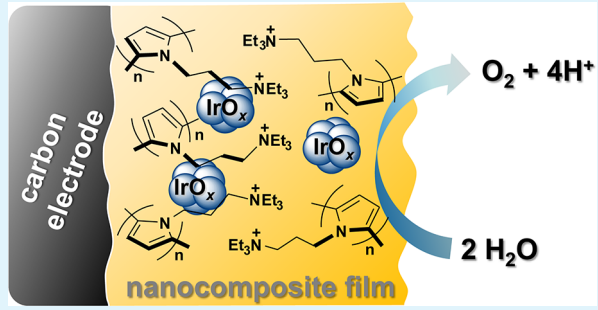

KEYWORDS: *iridium oxide, nanocomposites, electrode materials, electrocatalysis, oxygen evolution reaction*

1. INTRODUCTION

Global energy demand will roughly double by midcentury and triple by 2100. The success in meeting this energy challenge will largely depend on the design, research, and development of new technologies providing a solution for an abundant, clean and sustainable energy. Typically, the power generated from natural and renewable sources, including solar and wind, is undulating and intermittent, which requires energy storage because of its variability. Hydrogen has emerged as an attractive candidate for a clean fuel. Thus, an important step toward meeting this objective is to develop systems that can use an energy input to split water into hydrogen and oxygen, thereby providing an effective means for conversion and storage of energy from green and sustainable sources.[1] In this context, a highly desirable strategy is water electrolysis, a process which requires a complex proton-coupled multielectron oxidation of water to dioxygen with the release of four protons, and their subsequent reduction to dihydrogen.

The four-electron oxidation of water (reaction 1) is a pressing challenge;[1−9] it remains as a bottleneck because of its associated slow electrode kinetics.[10−13]

$$2H_2O \rightarrow 4H^+ + O_2 + 4e^- \quad (1)$$

Therefore, robust electrode materials for the electrocatalytic oxidation of water are required to produce oxygen efficiently, at high turnover rates and low overpotential. Noble and transition metal oxides at high valency remain the best catalysts for water oxidation.[14] Among these, hydrous iridium oxide ($IrO_x.nH_2O$) is one of the most efficient catalysts for the oxygen evolution reaction (OER) capable of operating over a wide pH range.

Iridium oxide can be synthesized in the form of nanoparticles and films,[14−29] using chemical or electrochemical techniques.[30] Broadly, chemical deposition techniques produce stable materials of low surface area, while the electrolytic oxides can have high surface area but often poor stability. Progress in the electrodeposition of stable and active iridium oxide thin films on different supports have been recently reported.[24,26,28]

A key factor in the performance of an electrocatalyst is its nanostructuration,[31,32] since efficiency is markedly enhanced by increasing the surface area-to-volume ratio.[33] However, decreasing the particle size to increase the surface area of the catalyst results in a reduction of their stability and can lead to aggregation. Aggregation of metal oxide catalyst particles can be in principle prevented by using an inorganic matrix[7,34] or a polymer coating.[35,36] Thus, to both improve performance (efficiency and stability) and to reduce the cost of iridium oxide-based catalysts for the OER, an appealing approach is to design nanocomposites. To date, two studies have demonstrated that nanostructuration of electrode materials based on iridium oxide can increase their catalytic efficiency for OER, but this work was restricted to the analytical scale.[27,29]

The modification of electrode surfaces with functionalized polypyrrole films containing cationic[37] or complexing[38,39] moieties provides a straightforward and efficient route allowing high loadings of metal species to be accumulated at electrode interfaces. The attractive features of polypyrrole-alkylammo-

Received: May 8, 2014
Accepted: July 21, 2014
Published: July 21, 2014

nium films are their easy and efficient electrochemical synthesis, their remarkable high stability when coated on various electrode surfaces, and overall their outstanding potential independent ion-exchange properties that allow binding of anionic metal salts and complexes.[37,40,41] The entrapped metal species can be subsequently electrochemically reduced to precipitate catalyst particles into the polyammonium matrix. Composite electrode materials consisting of poly(pyrrole-alkylammmonium) films containing nanoparticles of noble[40] and transition[41] metals, or a metal oxide like RuO_2,[37,42,43] have already demonstrated their potential in various electrocatalytic applications.

Following a similar strategy, we have recently described preliminary results on the straightforward all-electrochemical synthesis of iridium oxide-based polymer film modified electrodes. These were found to be very efficient for the electrocatalytic oxidation of arsenic(III) species in applications for trace arsenic removal.[44] Here, we report an extended study on the optimization of the electrosynthesis of nanostructured iridium oxide−polymer composite electrode materials, together with structural and redox characterizations of the new materials. The electrocatalytic activity of the composite materials toward water oxidation and oxygen evolution has been studied at the analytical scale using polymer modified microelectrodes, and also at macroelectrodes in bulk electrolysis experiments. In addition, the electrocatalytic performances of the IrO_x−polymer composite films were compared to those of regular electrosynthesized iridium oxide films.

2. EXPERIMENTAL SECTION

2.1. Chemicals and Reagents. (3-Pyrrol-1-yl-propyl)-triethylammonium tetrafluoroborate, denoted monomer **1** (Scheme 1), was prepared according to a previously reported procedure.[37]

Scheme 1. Pyrrole-Containing Monomer (1) Used in This Work

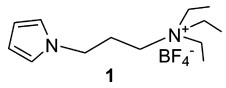

1

Potassium hexachloroiridate(III) (K_3IrCl_6, 99%, Aldrich), acetonitrile (Rathburn HPLC, grade S) and tetra-*n*-butylammonium perchlorate (TBAP, Fluka puriss) were used as received. Distilled water was obtained from an Elgastat water purification system (5 MΩ cm).

2.2. Electrodes, Electrochemical Cells, and Instrumentation. All electrochemical experiments were performed using a conventional three-electrode system. Electroanalytical experiments were performed using a CHI 660B electrochemical analyzer (CH Instruments). Electrosynthesis of nanocomposites and bulk electrolysis were carried out using an EGG PAR model 273 potentiostat. Potentials are referred to the Ag|AgCl (3 M KCl) or to the $Ag|Ag^+$ (10 mM in CH_3CN + 0.1 M TBAP) reference electrodes in aqueous and non aqueous electrolytes, respectively. For analytical experiments, glassy carbon microelectrodes (3 mm diameter) were polished with 1-μm diamond paste. Large-scale electrolyses were conducted on modified carbon foam electrodes (0.5 × 1 × 2 cm, porosity 100 ppi, from Electrosynthesis). Samples for microscopy characterization were deposited onto indium tin oxide (ITO) electrodes. All experiments were conducted at room temperature under an argon atmosphere.

2.3. Preparation of the Nanocomposite Film Modified Electrodes. *2.3.1. Electrosynthesis of Poly(pyrrole-alkylammonium).* Polymer films (denoted poly**1**) were grown by potentiostatic oxidative electropolymerization in unstirred solutions of monomer **1** (4 mM) in CH_3CN containing TBAP (0.1 M) as supporting electrolyte.[37,40] The extent of the polymerization was controlled through the anodic charge recorded during electrolysis. The amount of pyrrole units in the films, and thus the apparent surface coverage in ammonium units Γ_{N+} (mol cm^{-2}) were determined, after transfer of the modified electrodes into monomer-free CH_3CN electrolyte, from the integration of the polypyrrole oxidation wave recorded at low scan rate (10 mV s^{-1}), assuming that one in three pyrrole units is oxidized.[45] For the preparation of C|poly**1**-modified microelectrodes, films with Γ_{N+} ranging from 2.0×10^{-8} to 6.0×10^{-8} mol cm^{-2} were grown onto glassy carbon disc (3 mm diameter) electrodes by controlled potential oxidation carried out at E_{app} = 0.85 V vs $Ag|Ag^+$ (10^{-2} M), using polymerization charges from 0.5 to 2 mC. Prior to the incorporation of iridium oxide, the electroactivity of the polymer film was fully destroyed[46] by cycling the electrode potential several times between 0 and 1.6 V in a clean electrolyte. This allowed measurement of the intrinsic activity of the incorporated electrocatalyst uncomplicated by the redox response of the conducting polymer backbone. Modification of carbon foam electrodes was achieved by potentiostatic oxidative electropolymerization of monomer **1** in acetonitrile electrolyte at E_{app} = 0.9 V vs $Ag|Ag^+$ (10^{-2} M), using polymerization charges of 0.5 to 1.5 C. This process led to the deposition of a polymeric material onto the carbon foam containing about 1−3 μmol of ammonium groups (electrodeposition yield around 45%).

2.3.2. Electrodeposition of Iridium Oxide. Iridium(IV) oxide was electrosynthesized using two different processes, denoted Method A and Method B. As shown by structural characterizations described below, the electrodeposition of iridium oxide onto poly**1** film modified carbon or ITO electrodes led to the formation of nanostructured composite films where IrO_x nanoparticles are dispersed throughout the polymer matrix. For comparative structural, redox and catalytic studies, regular iridium oxide films were coated onto naked carbon and ITO electrodes using the same electrochemical procedures.

Method A was performed by potential cycling of the electrodes into an $Ir^{III}_2O_3{\cdot}xH_2O$ solution. The latter was prepared as follows according to a literature procedure:[19] 287 mg of K_3IrCl_6 (5.5×10^{-4} mol) was dissolved in 25 mL of 0.1 M aqueous HCl and the solution was stirred at 80 °C for 2 h under argon to afford a light brown solution of diaquotetrachloroiridate(III) ion (eq 2). In a second step, argon-purged aqueous 0.5 M NaOH was added to afford the air-sensitive solution of iridium(III) oxide $Ir_2O_3{\cdot}xH_2O$ (eq 3).

$$IrCl_6^{3-} \xrightarrow{0.1\,M\,HCl} Ir(OH)_2Cl_4^- \quad (2)$$

$$Ir(OH)_2Cl_4^- \xrightarrow{NaOH} Ir_2O_3{\cdot}xH_2O \quad (3)$$

Deposition of iridium(IV) oxide particles was achieved by electrochemical oxidation (eq 4) using an $Ir_2O_3{\cdot}xH_2O$ stock solution by scanning the potential from −0.4 to 1.1 V at 50 mV s^{-1} at polymer modified and naked electrodes. (see Figures S1A and S1B in Supporting Information).

$$Ir_2O_3{\cdot}xH_2O + 2OH^- \xrightarrow{Ox} 2IrO_x{\cdot}xH_2O + H_2O + 2e^- \quad (4)$$

Method B: iridium(IV) oxide was formed by acidic hydrolysis of $[Ir(OH)_6]^{2-}$ aqueous solutions, following the procedure described by Mallouk.[26] Iridium(IV) hydroxide was first prepared as follows according to literature recipes.[26,47] A 2 mM solution of K_3IrCl_6 in 0.1 M NaOH was slowly raised to 70 °C, then immediately cooled in an ice−water bath (eq 5).

$$IrCl_6^{3-} \xrightarrow[70°C]{NaOH} [Ir(OH)_6]^{2-} \quad (5)$$

In a second step, a 0.4 mM solution of $[Ir(OH)_6]^{2-}$ was prepared by dilution of this stock solution with 0.1 M NaOH. The pH was adjusted to 8 with aqueous HCl. Electrodeposition of iridium(IV) oxide onto naked or poly**1** film modified electrodes was carried out by electrochemical oxidation at 0.9 V of this $[Ir(OH)_6]^{2-}$ solution (eq 6).

$$[Ir(OH)_6]^{2-} \xrightarrow{H^+} IrO_x nH_2O \quad (6)$$

2.4. Atomic Force Microscopy Experiments. Samples for AFM measurements were prepared by electrodeposition of iridium oxide on

poly**1** films deposited on ITO-coated glass electrodes (1 cm^2). Electropolymerization of monomer **1** in acetonitrile electrolyte was performed at a controlled oxidation potential of 1.1 V vs Ag|Ag^+ (10^{-2} M), using charges of 28 mC (Γ_{N+} = 6.1 × 10^{-8} mol cm^{-2}). Iridium oxide was then electrodeposited onto poly**1** films (method B), using charges of 28 mC (Γ_{IrOx} = 3.6 × 10^{-8} mol cm^{-2}). For comparative studies, IrO_x was deposited in the same way onto a naked ITO electrode (Γ_{IrOx} = 4.7 × 10^{-8} mol cm^{-2}). AFM measurements were performed with a PicoPlus instrument (Molecular Imaging) equipped with a PicoScan controller and an AC-mode control box. The topography images were recorded with different scanning ranges and a tapping nose was used for imaging. AFM cantilevers with an aluminum coating (BudgetSensors Tap150Al-G) with a nominal spring constant of 5 N m^{-1} were used. The measurement frequency was set to 15% below the resonance frequency (about 150 kHz). Images were treated using Gwyddion program.

2.5. Transmission Electron Microscopy Experiments. TEM samples were prepared first by growing poly**1** films onto ITO-coated glass electrodes (1 cm^2) by oxidative electropolymerization of monomer **1** in acetonitrile electrolyte at 1.1 V vs Ag|Ag^+ (10^{-2} M) using a charge of 80 mC. Iridium oxide nanoparticles were then electroprecipitated into polymer films by cycling the modified ITO| poly**1** electrodes 10 times in an $Ir_2O_3.xH_2O$ solution (Method A). Poly**1**-IrO_x nanocomposite films were peeled off following soaking of the modified ITO electrode in liquid nitrogen, and a piece of film was deposited in a flat mold filled with epoxy resin. The resin was cured at 60 °C for 72 h. Cross sections through the thickness of the nanocomposites were obtained with a diamond knife at a thickness of 70 nm using a Leica UC6 microtome. The thin sections were collected onto a slotted pattern copper grid (type 75/300) and observed at 200 kV with a JEOL 2010 transmission electron microscope in the laboratory of "Laboratoire des Matériaux et du Génie Physique" (LMGP-CNRS 5628, INP-Minatec, Grenoble, France).

2.6. Analysis of Dioxygen and Hydrogen Peroxide. Real-time measurements of dissolved oxygen concentration coupled to water oxidation at poly**1**-IrO_x and IrO_x films modified carbon foam electrodes were made using a YSI Clark-type oxygen electrode immersed in the electrolytic solution. Prior to each set of experiments, the oxygen-permeable membrane was replaced to ensure a high quality response and complete electrical isolation of the Clark electrode from the bulk solution. The amount of oxygen evolved in the gas phase, above the liquid phase in the working compartment of the electrolysis cell, was quantified by gas chromatography using a PerkinElmer Autosystem XL Gas Chromatograph equipped with a 5 Å molecular sieve column (oven temperature =303 K) and a thermal conductivity detector (TCD), using argon as a carrier gas. Prior to each experiment, GC/TCD calibration was carried out by using oxygen of the air (20.95%) as reference.

The amount of hydrogen peroxide formed was determined at the end of each electrolysis experiment, from square wave voltammograms recorded at a 3 mm diameter Pt disc electrode (see Supporting Information, Figure S2A). The pulse amplitude was 80 mV, the potential step height was 1 mV, and the square-wave frequency was 10 Hz. H_2O_2 was determined from a calibration curve (Figure S2B), and also by means of the standard addition method.

3. RESULTS AND DISCUSSION

3.1. Electrosynthesis of Poly(pyrrole-alkylammonium)−Iridium Oxide Nanocomposite Electrode Materials. The composition of hydrous iridium oxide films, generally denoted IrO_x, implies a mixture of oxides and hydroxides with iridium predominantly in the Ir^{IV} state.[48] It is well-established that the electrochemical deposition of iridium oxide films on carbon, platinum, gold or conducting oxide-coated glass electrodes can be readily performed by oxidation from basic solutions of iridium oxides[19,22,44] and hydroxides.[20,26] In particular, the electrochemical oxidation of an $Ir^{III}_2O_3{\cdot}xH_2O$ solution leads to the formation of an insoluble hydrous iridium(IV) oxide (see Experimental, eq 4).[19] Moreover, since iridium oxide nanoparticles can be formed by acidic hydrolysis of $[Ir^{IV}(OH)_6]^{2-}$ (see Experimental Section, eq 6),[47] thin films of iridium(IV) oxide can be readily anodically grown onto various electrodes under oxidative induced acidic conditions due to water oxidation.[26]

We have recently described[44] that thin films of poly**1**−iridium oxide nanocomposite can be prepared by scanning Cl poly**1** film modified electrodes over the −0.4 to 1.1 V potential range in an $Ir_2O_3{\cdot}xH_2O$ solution for 10−25 consecutive cycles (Method A; see Figure S1B in Supporting Information). As for regular iridium oxide films electroprecipitated on naked carbon[19] (see Figure S1A in Supporting Information), 10−20 cycles are enough to obtain the best coatings. More cycles do not give a significant increase in the amount of electrodeposited iridium oxide.

To take better advantage from the excellent ion-exchange properties of the cationic poly**1** films, here we present another approach for the electrosynthesis of iridium oxide-based composite materials, by using the anionic $[Ir(OH)_6]^{2-}$ species as precursor. Thus, composite films were also synthesized by precipitation of IrO_x into poly**1** films by oxidation in the 0.9−1.0 V potential range into $[Ir(OH)_6]^{2-}$ solutions (Method B; see Experimental Section). In this case, we can expect a larger incorporation rate of iridium oxide in poly**1** films and a better nanostructuration of the resulting composite, therefore a higher catalytic activity of these electrode materials.

3.2. Electrochemical Characterization of Poly(pyrrole-alkylammonium)−Iridium Oxide Composite Film Modified Electrodes. When studied by cyclic voltammetry, iridium oxide-containing composite film modified electrodes prepared according to Method A (Figure 1A) or Method B (Figure 1B) exhibit a similar well-behaved and stable redox activity, in acidic and basic aqueous electrolytes. Taking into account that the electroactivity of the polymer matrix was purposely destroyed during the fabrication process (see the Experimental Section), the redox waves observed on the cyclic voltammograms are only due to iridium oxide species. This is confirmed by comparison with the redox features of pure iridium oxide film coated onto a naked carbon electrode, using for example Method B (Figure 1C). According to earlier works on the electrochemical behavior of iridium oxide films,[19,20,22,24,26,49] the peaks observed on the cyclic voltammetry curves recorded at various pH can be unambiguously assigned to the $Ir^{IV/III}$, $Ir^{V/IV}$ and $Ir^{VI/V}$ redox couples (see Figure 1A, for example). In addition, the large increase in the anodic currents observed at higher potentials is due to the electrocatalytic oxidation of water by $Ir^{VI}O_x$ species[24,26] formed in the nanocomposite film, as discussed in more detail below.

As observed for thin films of iridium oxide nanoparticles,[24,26,47,48] the potential of the different redox couples decreases linearly with increasing pH values. For example, the potential of the $Ir^{IV}O_x/Ir^{III}O_x$ wave decreases form 0.6 V at pH 1 (Figure 1, curves a) to −0.3 V at pH 13 (Figure 1, curves e). This corresponds to a decrease of about 75 mV per pH unit, suggesting that this wave involves removal of one electron/exchanged proton from the iridium center.[19,49]

The loading of the deposited iridium oxide Γ_{IrOx} was determined from the integration of the Ir^{III}/Ir^{IV} oxidation wave (see for example Figure 1A, and Figure S1C in Supporting Information) recorded at low scan rate (ν = 20 mV s^{-1}) after transfer of the modified electrode into clean aqueous electrolyte.

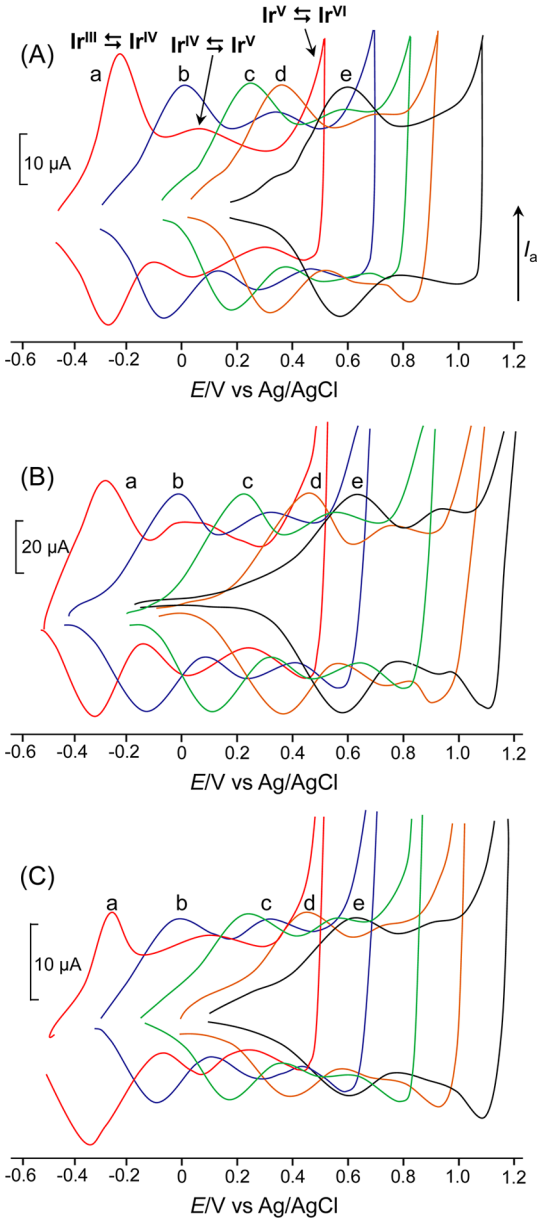

Figure 1. Cyclic voltammetry curves for different iridium oxide-based modified carbon disc electrodes (3 mm diameter) recorded at pH 13 (0.1 M NaOH; curves a), pH 10 (phosphate buffer; curves b), pH 7 (phosphate buffer and citric acid; curves c), pH 4 (phosphate buffer; curves d), and pH 1 (0.1 M HNO_3; curves e); scan rate 20 mV s^{-1}. (A) C|poly**1**-IrO_x electrode synthesized with Method A (Γ_{N+} = 4.3 × 10^{-8} mol cm^{-2}, Γ_{IrOx} = 3.6 × 10^{-8} mol cm^{-2}). (B) C|poly**1**-IrO_x electrode synthesized with Method B (Γ_{N+} = 8.3 × 10^{-8} mol cm^{-2}, Γ_{IrOx} = 7.3 × 10^{-8} mol cm^{-2}). (C) C|IrO_x electrode synthesized with Method B (Γ_{IrOx} = 3.1 × 10^{-8} mol cm^{-2}).

The electroprecipitation of iridium oxide into polypyrrole-alkylammonium films appeared more efficient than the coating of an oxide film on a naked electrode surface. With Method A, the electrodeposition of IrO_x in a poly**1** film is slightly larger than that onto a naked carbon surface. As an example, the amount of iridium oxide deposited into a poly**1** film after 10 consecutive cyclic voltammetry scans in an Ir_2O_3 solution (see Supporting Information, Figure S1B) reached 6 × 10^{-8} mol cm^{-2} (Figure S1C, curve b), while in the same experimental conditions the amount of the iridium oxide coated onto a naked carbon electrode (Figure S1A) was only of 4.9 × 10^{-8} mol cm^{-2} (Figure S1C, curve a).

As expected, Method B is much more efficient than Method A for the electrodeposition of iridium oxide into polypyrrole-alkylammonium films. In very similar experimental conditions, the amount of IrO_x electrodeposited using Method B, by oxidation at 1.0 V into a solution of $[Ir(OH)_6]^{2-}$, is more than twice as large in a poly**1** film (Γ_{IrOx} = 7.3 × 10^{-8} mol cm^{-2}, anodic charge passed 4.2 mC; Figure 1B) than onto a bare carbon surface (Γ_{IrOx} = 3.1 × 10^{-8} mol cm^{-2}, anodic charge passed 4.5 mC; Figure 1B). This result is due to the efficient incorporation and concentration by ion-exchange of the anionic iridium hydroxide precursor into the cationic poly(pyrrole-alkylammonium) matrix. Moreover Method B appeared more reproducible than Method A, probably because the solution of $Ir^{III}_2O_3 \cdot xH_2O$ used with Method A is highly air-sensitive,[19] contrary to the solution of $[Ir^{IV}(OH)_6]^{2-}$ used with Method B.

3.3. Structural Characterization of Poly(pyrrole-alkylammonium)–Iridium Oxide Films. Our preliminary investigations[44] have demonstrated that the electrodeposition of iridium oxide into poly(pyrrole-alkylammonium) results in the formation of a nanostructured composite. Transmission electron microscopy (TEM) of a cross-sectional area of a thin film (100 nm; Figure 2A) of iridium oxide–poly**1** composite

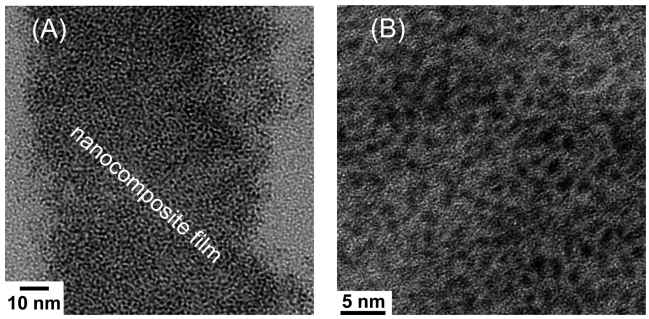

Figure 2. (A) TEM image of a cross-sectional view of a poly**1**-iridium oxide composite thin film; (B) enlargement of (A).

synthesized using Method A (see the Experimental Section for the preparation of the samples) reveals that iridium oxide particles with size ranging from 1–2 nm are well distributed throughout the composite film (Figure 2B).

AFM measurements in tapping mode were performed in order to study and to compare the surface morphologies of composite films and regular iridium oxide deposits, coated on ITO surfaces using Method B. Figure 3 shows topography images of the various surfaces. AFM imaging of the surface of bare ITO presented a homogeneous granular topology (Figure 3A) with a root-mean square roughness (r.m.s.) of 9 nm.

The electrodeposition of iridium oxide onto this naked ITO gave rise to a clear change in topology (Figure 3B), due to the formation on the surface of large aggregates of IrO_x particles with an average diameter from 100 to 200 nm (Figure 3E). This change was also reflected in the r.m.s. value, which was found to increase significantly to 53 nm.

After modification of the ITO surface with a poly(pyrrole-alkylammonium) film, the topography appeared nodular, typical of an electrodeposited poly**1** film,[40] and the r.m.s. roughness value increased significantly to 20 nm (Figure 3C). The deposition of iridium oxide onto the poly**1** film modified electrode resulted in a slight change in the roughness of the

dx.doi.org/10.1021/am5027852 | ACS Appl. Mater. Interfaces 2014, 6, 12852–12859

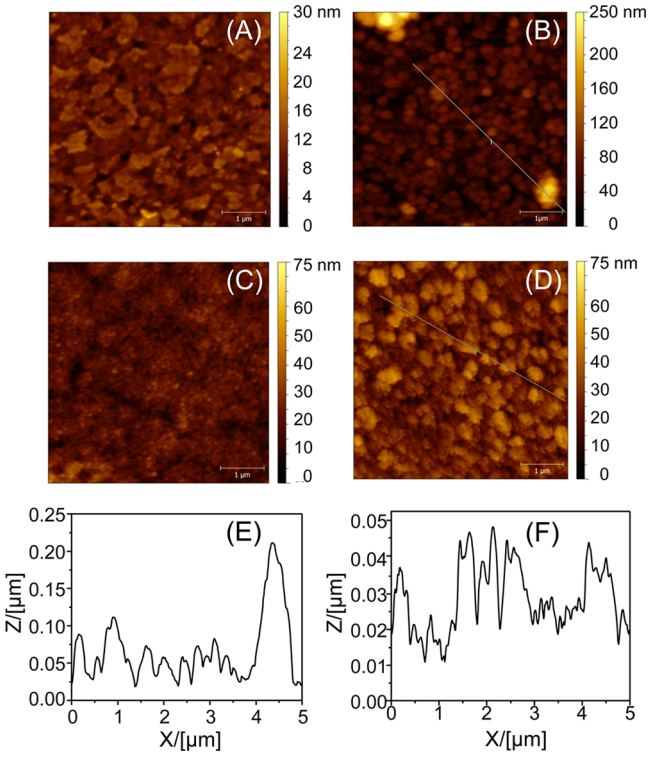

Figure 3. AFM images in tapping mode of (A) ITO naked surface; (B) ITO coated with IrO_x ($\Gamma_{IrOx} = 4.7 \times 10^{-8}$ mol cm^{-2}); (C) ITO coated with a poly**1** film ($\Gamma_{N+} = 6.1 \times 10^{-8}$ mol cm^{-2}); (D) ITO covered with poly**1**-IrO_x nanocomposite ($\Gamma_{N+} = 6.1 \times 10^{-8}$ mol cm^{-2}, $\Gamma_{IrOx} = 3.6 \times 10^{-8}$ mol cm^{-2}; (E) and (F) present section analysis of IrO_x film and poly**1**-IrO_x nanocomposite film coated onto ITO surfaces shown in (B) and (D), respectively; electrodeposition of iridium oxide was performed using Method B.

surface, the r.m.s. value increasing from 20 (Figure 3C) to 28 nm (Figure 3D). The very small increase in the r.m.s roughness value for the composite film is in agreement with the electrodeposition of iridium oxide into the poly**1** matrix, and not only on the polymer surface. A section analysis of the surface of the composite (Figure 3F) revealed the formation of smaller aggregates of IrO_x particles (average diameter from 25 to 50 nm) on the surface of the composite film, as compared to the larger aggregates obtained by electrodeposition of iridium oxide onto naked ITO (average diameter from 100 to 200 nm; see Figure 3E). Contrary to TEM analysis, AFM experiments does not allow to determine the size of the iridium oxide nanoparticles deposited into the polymer matrix. However, these results demonstrate that the electrodeposition of IrO_x into a poly(pyrrole-alkylammonium) film resulted in the formation of a more nanostructured composite, especially characterized by a homogeneous distribution of much smaller aggregates of IrO_x particles on its surface.

3.4. Electrocatalytic Water Oxidation at Clpoly1-IrO_x Modified Electrodes. All the electrocatalytic experiments have been conducted with electrode materials synthesized using Method B, which was found much more efficient and reproducible for the electrosynthesis of nanocomposite films. Cyclic voltammetry curves recorded with a rotating disc modified electrode (RDE) at varied pHs clearly show sharply rising anodic currents at high potentials (Figure 4A), corresponding to almost quantitative water oxidation and dioxygen evolution, as confirmed below by preparative scale electrolysis at large surface modified electrodes.

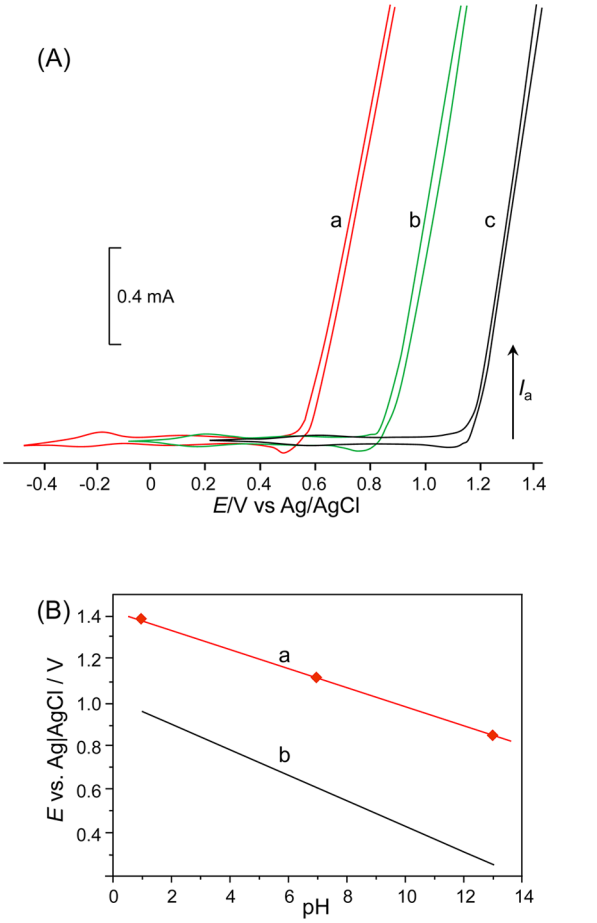

Figure 4. (A) Cyclic voltammetry curves for a rotating carbon disc electrode modified with a poly**1**-IrO_x film (synthesized with Method A: $\Gamma_{N+} = 4.3 \times 10^{-8}$ mol cm^{-2}, $\Gamma_{IrOx} = 3.6 \times 10^{-8}$ mol cm^{-2}) recorded at pH 13 (curve a), pH 7 (curve b), and pH 1 (curve c); $\omega = 1000$ rpm, $\nu = 20$ mV s^{-1}. (B) Overpotentials measured at 25 mA cm^{-2} at various pH (curve a, data from (A)) compared to the pH-dependent equilibrium potential of the OER (curve b).

This behavior is similar to that obtained at carbon electrode modified with films of iridium oxide nanoparticles.[24,26,47] For example, the current density for water oxidation at 1.2 V (pH 7) is about 100 mA cm^{-2} at a Clpoly**1**-IrO_x RDE modified electrode ($\Gamma_{IrOx} = 4 \times 10^{-8}$ mol cm^{-2}; 1000 rpm), which compares well with the result obtained by Murray and co-workers using a mesoporous IrO_x nanoparticles film under similar experimental conditions (91 mA cm^{-2} at 1.3 V, pH 7).[24]

Potentials for water oxidation at different pH values, measured at a current density of 25 mA cm^{-2} from the curves shown in Figure 4A, are depicted in Figure 4B (red dots, curve a) and compared to the thermodynamic potentials for the OER (Figure 4B, black curve b). In these experimental conditions, the poly**1**-IrO_x composite film modified electrode exhibited an overpotential for water oxidation varying from 0.4 to 0.5 V in 1 to 13 pH range.

Tafel plots for water oxidation (Figure 5) have been recorded in acidic (pH 1), neutral (pH 7) and basic (pH 13) electrolytes at Clpoly**1**-IrO_x (Figure 5, red curves) and ClIrO_x (Figure 5, black curves) anodes. Tafel slopes for the OER at various pH

dx.doi.org/10.1021/am5027852 | ACS Appl. Mater. Interfaces 2014, 6, 12852−12859

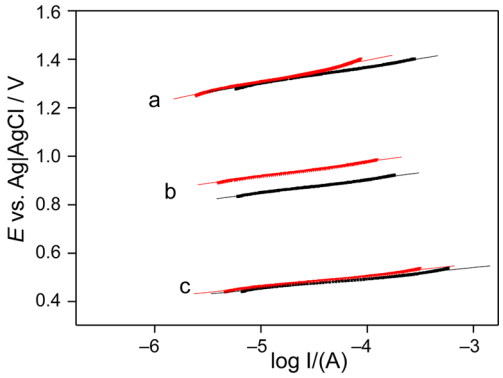

Figure 5. Tafel plots for the OER at C|poly**1**-IrO_x (red curves; 3 mm diameter, $\Gamma_{N+} = 5.5 \times 10^{-8}$ mol cm^{-2}, $\Gamma_{IrOx} = 3.1 \times 0^{-8}$ mol cm^{-2}) and at C|IrO_x (black curves; 3 mm diameter, $\Gamma_{IrOx} = 4.2 \times 10^{-9}$ mol cm^{-2}) electrodes, recorded at pH 1 (0.1 M H_2SO_4; curve a), pH 7 (phosphate buffer; curve b), and pH 13 (0.1 M NaOH; curve c); ω = 1000 rpm, ν = 20 mV s^{-1}.

are very similar for both types of modified electrode (Table 1). Tafel slopes are in the 30−60 mV dec^{-1} range, in agreement with that reported in the literature for regular iridium oxide thin films.[26,47] The average of the Tafel coefficients for these electrodes is also consistent with typical values calculated in the course of mechanistic studies for OER at various IrO_x-based electrodes.[30,50,51] These observations clearly point out that the catalytic activity of IrO_x nanoparticles toward water oxidation and dioxygen evolution is fully maintained when they are incorporated in the poly**1** matrix.

Table 1. Tafel Slopes for the OER Recorded at IrO_x and Poly1-IrO_x Film Modified Carbon Electrodes[a], at Various pH

electrode	pH	Tafel slope/mV dec^{-1}
C|poly**1**-IrO_x[b]	1[d]	31
C|IrO_x[c]	1	33
C|poly**1**-IrO_x[b]	7[e]	43
C|IrO_c	7[e]	41
C|poly**1**-IrO_x[b]	13[f]	52
C|IrO_x[c]	13[f]	58

[a]Synthesized with Method B. [b]$\Gamma_{N+} = 5.5 \times 10^{-8}$ mol cm^{-2}, $\Gamma_{IrOx} = 3.1 \times 10^{-8}$ mol cm^{-2}. [c]$\Gamma_{IrOx} = 4.2 \times 10^{-8}$ mol cm^{-2}. [d]0.1 M H_2SO_4. [e]Phosphate buffer. [f]0.1 M NaOH.

3.5. Electrocatalytic Water Oxidation at the Preparative Scale. The efficiency of the iridium oxide-based nanocomposite material for bulk oxidation of water at a macroscopic electrodes was evaluated using poly**1**-IrO_x modified carbon foam electrodes, and compared with the electrocatalytic activity of carbon foam modified with regular IrO_x films. For both types of anode, the electrodeposition of IrO_x onto naked or poly**1** modified carbon foam electrode was performed using Method B. Large-scale oxidation of water was conducted in a three-compartment cell, at 1.3 V (pH 7) or 1.8 V (pH 1) versus the Ag|AgCl reference electrode. Oxygen was analyzed during the course of the electrolyses in the gas phase by gas chromatography and in the solution phase using a Clark electrode (see Experimental Section). Electrolyses were arbitrarily stopped after the passage of a fixed charge of 50 C, and the solutions analyzed for hydrogen peroxide by square wave voltammetry recorded at a Pt electrode (see Experimental Section). The main results of a series of electrolysis performed at pH 7 and at pH 1 are listed in Table 2.

Under these experimental conditions, the composite films presented a better catalytic activity and a higher operational stability than regular oxide films. For example, at pH 7 the initial catalytic current recorded with a pure oxide film (16 mA; Table 2, entry 1) was significantly lower than that obtained at C|poly**1**-IrO_x anodes (26 mA) containing the same (0.1 μmol; entry 3), or even lower catalyst loading (0.04 mmol; entry 2). These results were confirmed by experiments conducted at pH 1, where a higher initial current was obtained at a C|poly**1**-IrO_x modified electrode (62 mA; entry 5), as compared to a C|IrO_x anode (45 mA; entry 4) containing a higher amount of catalytic oxide. The higher efficiency of the composite material synthesized with a lower amount of iridium oxide (Table 2, entry 5) can be explained by higher catalytic surface area-to-volume ratio, due to the nanostructuration of the composite as suggested by the TEM and AFM characterizations.

In all experiments, we observed a significant drop in the initial current of each electrolysis. After the consumption of a few coulombs, the catalytic current remained almost stable. However, an important feature of the poly**1**-IrO_x composite film is an improved operational stability. For example, under comparable conditions (pH 7) after the consumption of 50 C, we observed a decrease in the catalytic current of 20% (entry 3), while with a C|IrO_x modified electrode containing the same amount of catalyst the best result was a decrease of 25% in the electrolysis current (Table 2, entry 5). Moreover, in acidic electrolyte (pH 1). the composite material appeared much more stable (decrease in the catalytic current: 15%, entry 5) than a pure oxide film (decrease in the catalytic current: 55%, entry 4).

An interesting point is that the amount of hydrogen peroxide, formed by a noncatalytic 2-electron process, is significantly lower at the C|poly**1**-IrO_x modified electrodes (2%; entries 2 and 3) than on a regular oxide film (5%; entry 1) when the electrolysis are performed at pH 7. This result could be explained by the fact that the polymer film partially blocks

Table 2. Results for the Electrocatalytic Oxidation of H_2O at Pure IrO_x and poly1-IrO_x Film Modified Electrodes

entry	pH	E_{app}/V[a]	electrode[b]	poly**1**/μmol	IrO_x/μmol	I_i/mA[c]	I_f/mA[d]	O_2 yield/%[e]	H_2O_2 yield/%[f]
1	7[g]	1.3	C|IrO_x	-	0.1	16	12	95	5
2	7[g]	1.3	C|poly**1**-IrO_x	0.6	0.04	26	6	97	2
3	7[g]	1.3	C|poly**1**-IrO_x	0.75	0.1	26	21	99	2
4	**1**[h]	1.8	C|IrO_x	-	0.12	45	20	99	trace
5	**1**[h]	1.8	C|poly**1**-IrO_x	0.6	0.07	62	53	99	trace

[a]Applied electrolysis potential, vsAg|AgCl (3 M KCl). [b]1 cm^3 of modified carbon foam (100 ppi); electrodeposition of IrO_x was performed using Method B. [c]Initial current. [d]Final current, measured after the consumption of 50 C. [e]Total yield of produced O_2, measured in the electrolyte with a Clark electrode and in the gas phase by GC. [f]Determined by SWV at a Pt disc electrode. [g]Phosphate buffer. [h]0.1 M H_2SO_4.

direct access to the carbon surface, and consequently the 2-electron oxidation of water. The very low amount of hydrogen peroxide measured with both kind of electrodes when electrolysis was performed at pH 1 (entries 4 and 5) is probably due to the higher oxidation potential (1.8 V) applied in these experimental conditions, which leads to the oxidative decomposition of H_2O_2.[52]

4. CONCLUSION

In conclusion, we have demonstrated that iridium oxide-polymer nanocomposites synthesized using a straightforward all-electrochemical strategy, by precipitation of iridium oxide nanoparticles into a poly(pyrrole-alkylammonium) matrix, are efficient electrode nanomaterials for electrocatalytic water oxidation in an OER. Electroanalytical investigations have shown that the electrocatalytic activity of iridium oxide nanoparticles is fully maintained when they are incorporated in the polymer matrix. Bulk electrocatalytic oxidation of water at carbon foam modified macroscopic electrodes has shown that the composite films display a high catalytic activity and a reasonable operational stability, exceeding that of regular iridium oxide films containing a higher loading of catalyst. The enhanced catalytic performances of the composite electrode materials can be attributed to their nanostructure, as shown by TEM and AFM characterization.

Finally, we note that the very simple strategy reported herein for the assembly of composite films using alkylammonium functionalized electropolymers might well be extended to emerging electrocatalyst for water splitting based on earth-abundant elements.

■ ASSOCIATED CONTENT

Ⓢ Supporting Information

Cyclic voltammograms for electrosynthesis and characterization of IrO_x and composites films using Method A. DPV and calibration curves for H_2O_2 analysis. This material is available free of charge via the Internet at http://pubs.acs.org.

■ AUTHOR INFORMATION

Corresponding Author

*E-mail: Jean-Claude.Moutet@ujf-grenoble.fr. Fax: +33-476-514-267. Phone: +33-476-514-481.

Notes

The authors declare no competing financial interest.

■ ACKNOWLEDGMENTS

The authors thank for funding the French National Agency for Research (Programme LABEX ARCANE, project no. ANR-11-LABX-003). We acknowledge the support from the ICMG FR 2607, and its Chemistry Nanobio Platform for AFM measurements. The authors are grateful to Dr. Isabelle Pignot-Paintrand, Hugues Bonnet and Prof. Pierre Labbé, for their help for the structural characterizations of the composite materials. Special thanks go to Prof. C. J. Pickett, the University of East Anglia, for a critical reading of the manuscript.

■ REFERENCES

(1) Cook, T. R.; Dogutan, D. K.; Reece, S. Y.; Surendranath, Y.; Teets, T. S.; Nocera, D. C. Solar Energy Supply and Storage for the Legacy and Nonlegacy Worlds. *Chem. Rev.* **2010**, *110*, 6474−6502.

(2) Blakemore, J. D.; Schley, N. D.; Balcells, D.; Hull, J. F.; Olack, G. W.; Incarvito, C. D.; Eisenstein, O.; Brudvig, G. W.; Crabtree, R. H. Half-Sandwich Iridium Complexes for Homogeneous Water-Oxidation Catalysis. *J. Am. Chem. Soc.* **2010**, *132*, 16017−16029.

(3) Brimblecombe, R.; Swiegers, G. F.; Dismukes, G. C.; Spiccia, L. Sustained Water Oxidation Photocatalysis by a Bioinspired Manganese Cluster. *Angew. Chem., Int. Ed.* **2008**, *47*, 7335−7338.

(4) Chen, H. Y.; Faller, J. W.; Crabtree, R. H.; Brudvig, G. W. Dimer-of-Dimers Model for the Oxygen-Evolving Complex of Photosystem II. Synthesis and Properties of $[Mn^{IV}_4O_5(terpy)_4(H_2O)_2](ClO_4)_6$. *J. Am. Chem. Soc.* **2004**, *126*, 7345−7349.

(5) Concepcion, J. J.; Jurss, J. W.; Templeton, J. L.; Meyer, T. J. Mediator-Assisted Water Oxidation by the Ruthenium "Blue Dimer" cis,cis-$[(bpy)_2(H_2O)RuORu(OH_2)(bpy)_2]^{4+}$. *Proc. Natl. Acad. Sci. U.S.A.* **2008**, *105*, 17632−17635.

(6) Dincă, M.; Surendranath, Y.; Nocera, D. G. Nickel-Borate Oxygen-Evolving Catalyst that Functions Under Benign Conditions. *Proc. Natl. Acad. Sci. U.S.A.* **2010**, *107*, 10337−10341.

(7) Jiao, F.; Frei, H. Nanostructured Manganese Oxide Clusters Supported on Mesoporous Silica as Efficient Oxygen-Evolving Catalysts. *Chem. Commun.* **2010**, *46*, 2920−2922.

(8) Kanan, M. W.; Nocera, D. G. In Situ Formation of an Oxygen-Evolving Catalyst in Neutral Water Containing Phosphate and Co^{2+}. *Science* **2008**, *321*, 1072−1075.

(9) Yin, Q.; Tan, J. M.; Besson, C.; Geletii, Y. V.; Musaev, D. G.; Kuznetsov, A. E.; Luo, Z.; Hardcastle, K. I.; Hill, C. L. A Fast Soluble Carbon-Free Molecular Water Oxidation Catalyst Based on Abundant Metals. *Science* **2010**, *328*, 342−345.

(10) Surendranath, Y.; Dincă, M.; Nocera, D. G. Electrolyte-Dependent Electrosynthesis and Activity of Cobalt-Based Water Oxidation Catalysts. *J. Am. Chem. Soc.* **2009**, *131*, 2615−2620.

(11) Morris, N. D.; Suzuki, M.; Mallouk, T. E. Kinetics of Electron Transfer and Oxygen Evolution in the Reaction of $[Ru(bpy)_3]^{3+}$ with Colloidal Iridium Oxide. *J. Phys. Chem. A* **2004**, *108*, 9115−9119.

(12) Hoertz, P. G.; Kim, Y.-I.; Youngblood, W. J.; Mallouk, T. E. Bidentate Dicarboxylate Capping Groups and Photosensitizers Control the Size of IrO_2 Nanoparticle Catalysts for Water Oxidation. *J. Phys. Chem. B* **2007**, *111*, 6845−6856.

(13) Youngblood, W. J.; Lee, S.-H. A.; Kobayashi, Y.; Hernandez-Pagan, E. A.; Hoertz, P. G. T.; Moore, T. A.; Moore, A. L.; Gust, D.; Mallouk, T. E. Photoassisted Overall Water Splitting in a Visible Light-Absorbing Dye-Sensitized Photoelectrochemical Cell. *J. Am. Chem. Soc.* **2009**, *131*, 926−927.

(14) McCrory, C. C. L.; Jung, S.; Peters, J. C.; Jaramillo, T. F. Benchmarking Heterogeneous Electrocatalysts for the Oxygen Evolution Reaction. *J. Am. Chem. Soc.* **2013**, *135*, 16977−16987.

(15) Harriman, A.; Thomas, J. M.; Millward, G. R. Catalytic and Structural Properties of Iridium-Iridium Dioxide Colloids. *New J. Chem.* **1987**, *11*, 757−762.

(16) Harriman, A.; Nahor, G. S.; Mosseri, S.; Neta, P. Iridium Oxide Hydrosols as Catalysts for the Decay of Zinc Phorphyrin Radical Cations in Water. *J. Chem. Soc., Faraday Trans.* **1988**, *84*, 2821−2829.

(17) Nahor, G. S.; Neta, P.; Hambright, P.; Thompson, A. N., Jr; Harriman, A. Metalloporphyrin-Sensitized Photoxidation of Water to Oxygen on the Surface of Colloidal Iridium Oxides: Photochemical and Pulse Radiolytic Studies. *J. Phys. Chem.* **1989**, *93*, 6181−6187.

(18) Yamanaka, K. Anodically Electrodeposited Iridium Oxide films (AEIROF) from Alkaline Solutions for Electrochromic Display Devices. *Jpn. J. Appl. Phys.* **1989**, *28*, 632−637.

(19) Baur, J. E.; Spaine, T. W. Electrochemical Deposition of Iridium(IV) Oxide from Alkaline Solutions of Iridium(III) Oxide. *J. Electroanal. Chem.* **1998**, *443*, 208−216.

(20) Petit, M. A.; Plichon, V. Anodic Electrodeposition of Iridium Oxide Films. *J. Electroanal. Chem.* **1998**, *444*, 247−252.

(21) Morris, N. D.; Mallouk, T. E. A High-Throughput Optical Screening Method for the Optimization of Colloidal Water Oxidation Catalysts. *J. Am. Chem. Soc.* **2002**, *124*, 11114−11121.

(22) Yagi, M.; Tomita, E.; Kuwabara, T. Remarkably High Activity of Electrodeposited IrO_2 Film for Electrocatalytic Water Oxidation. *J. Electroanal. Chem.* **2005**, *579*, 83−88.

(23) Nakamura, R.; Frei, H. Visible Light Driven Water Oxidation by Ir Clusters Coupled to Single Cr Centers in Mesoporous Silica. *J. Am. Chem. Soc.* **2006**, *128*, 10668−10669.
(24) Nakagawa, T.; Beasley, C. A.; Murray, R. W. Efficient Electro-Oxidation of Water Near its Reversible Potential by a Mesoporous IrO_x Nanoparticle Film. *J. Phys. Chem. C* **2009**, *113*, 12958−12961.
(25) Nakagawa, T.; Bjorge, N. S.; Murray, R. W. Electrogenerated IrO_x Nanoparticles as Dissolved Redox Catalysts for Water Oxidation. *J. Am. Chem. Soc.* **2009**, *131*, 15578−15579.
(26) Zhao, Y.; Vargas-Barbosa, N. M.; Hernandez-Pagan, E. A.; Mallouk, T. E. Anodic Deposition of Colloidal Oxide Thin Films from Hexahydroxyiridate(IV) Solutions. *Small* **2011**, *7*, 2087−2093.
(27) Ortel, E.; Reier, T.; Strasser, P.; Kraehnert, R. Mesoporous IrO_2 Films Templated by PEO-PB-PEO Block-Copolymers: Self-Assembly, Crystallization Behavior, and Electrocatalytic Performance. *Chem. Mater.* **2011**, *23*, 3201−3209.
(28) Blakemore, J. D.; Schley, N. D.; Kushner-Lenhoff, M. N.; Winter, A. W.; D'Souza, F.; Crabtree, R. H.; Brudvig, G. W. Comparison of Amorphous Iridium Water-Oxidation Electrocatalysts Prepared from Soluble Precursors. *Inorg. Chem.* **2012**, *51*, 7749−7763.
(29) Chuang, M.-C.; Ho, J. A. Efficient Electrocatalytic Oxidation of Water: Minimization of Catalyst Loading by an Electrostatic Assembly of Hydrous Iridium Oxide Colloids. *RSC Adv.* **2012**, *2*, 4092−4096.
(30) Guerrini, E.; Chen, H.; Trasatti, S. Oxygen Evolution on Aged IrO_x/Ti Electrodes in Alkaline Solutions. *J. Solid. State Electrochem.* **2007**, *11*, 939−945.
(31) Centi, G.; Perathoner, S. The Role of Nanostructure in Improving the Performance of Electrodes for Energy Storage and Conversion. *Eur. J. Inorg. Chem.* **2009**, 3851−3878.
(32) Menzel, N.; Ortel, E.; Kraehnert, R.; Strasser, P. Electrocatalysis Using Porous Nanostructured Materials. *ChemPhysChem* **2012**, *13*, 1385−1394.
(33) Esswein, A. J.; McMurdo, M. J.; Ross, P. N.; Bell, A. T.; Tilley, T. D. Size-Dependant Activity of Co_3O_4 Nanoparticles Anodes for Alkaline Water Electrolysis. *J. Phys. Chem. C* **2009**, *113*, 15068−15072.
(34) Jiao, F.; Frei, H. Nanostructured Cobalt Oxide Clusters in Mesoporous Silica as Efiicient Oxygen-Evolving Catalysts. *Angew. Chem., Int. Ed.* **2009**, *48*, 1841−1844.
(35) Kim, Y.-Y.; Hore, K.; Hall, S. R.; Walsh, D. Controlled Nanoparticle Formation by Enzymatic Deshelling of Biopolymer-Stabilized Nanosuspensions. *Small* **2009**, *5*, 913−918.
(36) Kim, Y.-Y.; Meldrum, F. C.; Walsh, D. Biopolymer Stabilized Nanoparticles as Co-Catalysts for Photocatalytic Water Oxidations. *Polym. Chem.* **2011**, *2*, 1375−1379.
(37) Cosnier, S.; Deronzier, A.; Moutet, J.-C.; Roland, J.-F. Alkylammonium and Pyridinium Group-Containing Polypyrroles, a New Class of Electronically Conducting Anion-Exchange Polymers. *J. Electroanal. Chem.* **1989**, *271*, 69−81.
(38) Heitzmann, M.; Brovelli, F.; Basaez, L.; Bucher, C.; Limosin, D.; Pereira, E.; Rivas, B. L.; Royal, G.; Saint-Aman, E.; Moutet, J.-C. Voltammetric Sensing of Trace Metals at a Polymalonic Acid Film Modified Carbon Electrode. *Electroanalysis* **2005**, *17*, 1970−1976.
(39) Heitzmann, M.; Bucher, C.; Moutet, J.-C.; Pereira, E.; Rivas, B. L.; Royal, G.; Saint-Aman, E. Complexation of Poly(EDTA-like) Film Modified Electrodes: Application to Metal Cations Electroanalysis. *Electrochim. Acta* **2007**, *52*, 3082−3087.
(40) De Oliveira, I. M. F.; Moutet, J.-C.; Hamar-Thibault, S. Electrocatalytic Hydrogenation Activity of Palladium and Rhodium Microparticles Dispersed in Alkylammonium- and Pyridinium-Substituted Polypyrrole Films. *J. Mater. Chem.* **1992**, *2*, 167−173.
(41) Zouaoui, A.; Stephan, O.; Carrier, M.; Moutet, J.-C. Electrodeposition of Copper into Functionalized Polypyrrole Films. *J. Electroanal. Chem.* **1999**, *474*, 113−122.
(42) Rivera, J. F.; Bucher, C.; Saint-Aman, E.; Rivas, B. L.; Aguirre, M. C.; Sánchez, J. A.; Pignot-Paintrand, I.; Moutet, J.-C. Removal of Arsenite by Coupled Electrocatalytic Oxidation at Polymer-Ruthenium Oxide Nanocomposite and Polymer-Assisted Liquid Phase Retention. *Appl. Catal., B* **2013**, *129*, 130−136.
(43) Cosnier, S.; Deronzier, A.; Roland, J.-F. Electrocatalytic Oxidation of Alcohols on Carbon Electrodes Modified by Functionalized Polypyrrole-RuO_2 Films. *J. Mol. Catal.* **1992**, *71*, 303−315.
(44) Rivera, J. F.; Pignot-Paintrand, I.; Pereira, E.; Rivas, B. L.; Moutet, J.-C. Iridium Oxide-Polymer Nanocomposite Thin Films for Electrocatalytic Oxidation of Arsenic(III). *Electrochim. Acta* **2013**, *110*, 465−476.
(45) Deronzier, A.; Moutet, J.-C. Polypyrrole Films Containing Metal Complexes: Syntheses and Applications. *Coord. Chem. Rev.* **1996**, *147*, 339−371 , and references therein..
(46) Rosseinsky, D. R.; Morse, N. J.; Slade, R. C. T.; Hix, G. B.; Mortimer, R. J.; Walton, D. J. Mechanisms of the Chemical and Electrochemical Polymerizations of Pyrrole Compared by Product Spectrometry and Conductivity Loss Effected by Pyridine Inhibition or by Over-Oxidation. *Electrochim. Acta* **1991**, *36*, 733−738.
(47) Zhao, Y.; Hernandez-Pagan, E. A.; Vargas-Barbosa, N. M.; Dysart, J. L.; Mallouk, T. E. A High Yield Synthesis of Ligand-Free Iridium Oxide Nanoparticles with High Electrocatalytic Activity. *J. Phys. Chem. Lett.* **2011**, *2*, 402−406.
(48) Juodkazyté, J.; Šebeka, B.; Valsiunas, I.; Juodkasis, K. Iridium Anodic Oxidation to Ir(III) and Ir(IV) Hydrous Oxides. *Electroanalysis* **2005**, *17*, 947−952.
(49) Salimi, A.; Hyde, M. E.; Banks, C. E.; Compton, R. G. Boron Doped Diamond Electrode Modified with Iridium Oxide for Amperometric Detection of Ultra Trace Amounts of Arsenic(III). *Analyst* **2004**, *129*, 9−14.
(50) Martelli, G. N.; Ornelas, R.; Faita, G. Deactivation Mechanisms of Oxygen Evolving Anodes at High Current Densities. *Electrochim. Acta* **1994**, *39*, 1551−1558.
(51) Hu, J.-M.; Zhang, J.-Q.; Cao, C.-N. Oxygen Evolution Reaction on IrO_2-Based DSA® Type Electrodes: Kinetics Analysis of Tafel Lines and EIS. *Int. J. Hydrogen Energy* **2004**, *29*, 791−797.
(52) Qiang, Z.; Chang, J.-H.; Huang, C.-P. Electrochemical Generation of Hydrogen Peroxide from Dissolved Oxygen in Acidic Solutions. *Water Res.* **2002**, *36*, 85−94.